particles

Tracked for Impact Factor

Indexed in: Scopus

Article

Centrality Selection Effect on Elliptic Flow Measurements in Relativistic Heavy-Ion Collisions at NICA Energies

Dim Idrisov, Petr Parfenov and Arkadiy Taranenko

Special Issue

Selected Papers from "Physics Performance Studies at FAIR and NICA"

Edited by

Prof. Dr. Peter Senger, Prof. Dr. Arkadiy Taranenko and Prof. Dr. Ilya Selyuzhenkov

MDPI

https://doi.org/10.3390/particles6020028

particles

MDPI

Article

Centrality Selection Effect on Elliptic Flow Measurements in Relativistic Heavy-Ion Collisions at NICA Energies

Dim Idrisov [1,*], Petr Parfenov [1,2] and Arkadiy Taranenko [1,3]

[1] MEPhI, National Research Nuclear University, Kashirskoe Highway 31, Moscow 115409, Russia; arkadij71@gmail.com (A.T.)
[2] Institute for Nuclear Research of the Russian Academy of Sciences, Moscow 119991, Russia
[3] Veksler and Baldin Laboratory of High Energy Physics at Joint Institute for Nuclear Research, Dubna 141980, Russia
* Correspondence: idrisov.dim@mail.ru

Abstract: The elliptic flow (v_2) of produced particles is one of the important observables sensitive to the transport properties of the strongly interacting matter created in relativistic heavy-ion collisions. Detailed differential measurements of v_2 are also foreseen in the future Multi-Purpose Detector (MPD) experiment at the Nuclotron based Ion Collider fAcility (NICA) at collision energies $\sqrt{s_{NN}}$ = 4–11 GeV. Elliptic flow strongly depends on collision geometry, defined by the impact parameter b. Usually b is an input to theoretical calculations and can be deduced from experimental observables in the final state using the centrality procedure. In this work, we investigate the influence of the choice of centrality procedure on the elliptic flow measurements at NICA energies.

Keywords: elliptic flow, heavy-ion collisions; centrality; MPD experiment; NICA energies

Citation: Idrisov, D.; Parfenov, P.; Taranenko, A. Centrality Selection Effect on Elliptic Flow Measurements in Relativistic Heavy-Ion Collisions at NICA Energies. *Particles* **2023**, *6*, 497–514. https://doi.org/10.3390/particles6020028

Academic Editor: Armen Sedrakian

Received: 23 March 2023
Revised: 18 April 2023
Accepted: 20 April 2023
Published: 26 April 2023

1. Introduction

The main purpose of the MPD detector at NICA is to explore the phase diagram of the strongly interacting matter in the region of high net-baryon densities [1]. Anisotropic collective flow is one of the most important observables to probe the equation of state and transport properties of matter created in relativistic heavy-ion collisions [2]. It can be quantified according to the Fourier coefficients v_n in the expansion of the particle azimuthal distribution relative to the collision symmetry plane given by the angle Ψ_n:

$$dN/d\phi \propto 1 + \sum_{n=1} 2v_n \cos(n(\phi - \Psi_n)), \quad (1)$$

where n is the order of the harmonic, and ϕ is the azimuthal angle of a particle. The coefficients v_n can be calculated as $v_n = \langle \cos[n(\varphi - \Psi_n)] \rangle$, where the brackets denote the average over the particles and events. The elliptic flow (v_2) is one of the most extensively studied observables in relativistic nucleus–nucleus collisions and it has been measured in different experiments in the last three decades [3]. The detailed measurements of v_2 of various hadrons produced in relativistic heavy-ion collisions at the Relativistic Heavy-Ion Collider (RHIC) and at the Large Hadron Collider (LHC) played an essential role in the discovery of the strongly coupled Quark-Gluon Matter (QGM) [4,5]. The elliptic flow signal strongly depends on collision geometry and viscous hydrodynamic studies suggest that v_2 stems from the evolution of the medium in the presence of initial-state anisotropies, determined by the eccentricity ε_2 of the overlap zone in nucleus–nucleus collisions. The v_2 signal is recognized to be almost linearly correlated to ε_2 : $v_2 = k_2 \times \varepsilon_2$ [5–7]. The coefficient k_2 encodes the medium response, which is sensitive to the temperature (T) dependent specific shear viscosity (i.e., the ratio of shear viscosity to entropy density $\eta/s(T)$) of strongly interacting system produced in the collisions [6–8]. Thus, the comparison of viscous hydrodynamical model calculations to the v_2/ε_2 for various collision centralities is commonly employed

to estimate the average $\eta/s(T)$ over the system's evolution [5,8]. The impact parameter b, defined as the transverse distance between the centers of the two colliding nuclei, is the best variable that can be used to define the collision centrality and a key input to most theoretical calculations of heavy-ion collisions. However, it can not be directly measured in experiments [9]. There, the heavy-ion collisions can be characterized by the measured multiplicities N_{ch} of the produced particles or by the forward (backward) rapidity energy E_{sp}, which is an approximation for the number of projectile (target) spectators. The centrality procedure is based on the correlation between measured N_{ch} (E_{sp}) and b, which can be deduced by fitting a specific model of particle production to the experimental data [10]. Usually, the correlation between the impact parameter b and the multiplicity N_{ch} is determined using the Monte-Carlo Glauber (MC Glauber) method combined with a simple particle production model [11]. The modeled multiplicity is assumed to be a function of the number of participating nucleons (N_{part}) and the number of binary interactions between nucleons (N_{coll}), which one obtains from the output of the MC Glauber model. The particle multiplicity distribution N_{ch}^{fit} can then be fitted to the experimentally measured one [12,13]. Centrality classes are defined by sharp cuts on N_{ch} and the corresponding mean values of $\langle b \rangle$ for each class determined from MC Glauber events. Although this approach seems to be well established, it may suffer from large systematic uncertainties at low multiplicities and assumptions about the particle production mechanism [10]. Recently, a new model-independent (Γ-fit) method for reconstructing the impact parameter distributions was proposed [14]. The main assumption is that the fluctuations of the N_{ch} used to determine the centrality at a fixed impact parameter b follow a gamma distribution [15].

In this work, we investigate the influence of the choice of centrality procedure on the elliptic flow measurements at NICA energies: $\sqrt{s_{NN}}$ = 4–11 GeV [16]. To address this issue, Au+Au collisions were simulated using Ultra-relativistic Quantum Molecular Dynamics (UrQMD) [17] and A Multi-Phase Transport (AMPT) [18] models. The elliptic flow results from events binning with the Γ-fit, and MC Glauber methods are compared to those with the true impact parameter from the models.

The paper is organized as follows. Section 2 briefly describes the used transport models (UrQMD and AMPT), while Section 3 discusses the MC Glauber and Γ-fit methods for centrality determination. Section 4 discusses the procedures used to determine the elliptic flow coefficient v_2. The effects of centrality filters on v_2 results are presented and discussed in Section 5. Finally, a summary is given in Section 6.

2. A Brief Description of the Models

In this work, the relativistic Au+Au collisions at $\sqrt{s_{NN}}$ = 5, 7.7 and 11.5 GeV are simulated by the string melting (SM) version of the AMPT [18] and the cascade version of the UrQMD [17] (version 3.4) models. The string-melting version of the hybrid AMPT model includes the QGM formation and incorporates both partonic and hadronic interactions, while the cascade version of the UrQMD model only takes the hadronic interactions into account (no QGM formation). The choice of these models is based on a detailed comparison of modern model approaches to existing measurements of the elliptic flow of hadrons in Au + Au collisions at energies close to the NICA range $\sqrt{s_{NN}}$ = 4-11 GeV [16,19,20]. The published v_2 results for Au+Au collisions at $\sqrt{s_{NN}}$ = 4.5, 7.7 and 11.5 GeV were obtained from the Beam Energy Scan program of the STAR experiment at RHIC [20–22]. Figure 1 shows the comparison of the p_T-differential v_2 of charged hadrons between different transport models and STAR published data [20] (blue solid circles) in the 20-30% central Au+Au collisions at $\sqrt{s_{NN}}$ = 7.7 GeV. The event plane and centrality in the analysis of the model events were determined in the same way as in the real STAR data analysis. An elliptic flow analysis was also performed in the same way using the η-sub event plane method. See [16,20] for further details. The left panel of Figure 1 represents the results for hybrid models with QGM formation: 3D viscous hydro + hadronic cascade vHLLE+UrQMD model [23,24] (open circles) and string melting version of AMPT SM [18] (open boxes). Both models provide a relatively good description of the published $v_2(p_T)$ results of charged hadrons.

However, the following models: UrQMD [17], DCM-QGSM-SMM [25], JAM [26], and SMASH [27], which only take the hadronic interactions into account (no QGM formation), significantly underestimate the published v_2 values. See the right panel of Figure 1 for more At an energy $\sqrt{s_{NN}}$ = 4.5 GeV, the hadronic cascade mode of the JAM and UrQMD models can provide a relatively good description of the published STAR $v_2(p_T)$ results for charged pions and protons. See [19] for the details. This may indicate that at energies $\sqrt{s_{NN}} \leq$ 4–6 GeV, the hadron gas phase dominates and models based on only hadron transport can be used to describe the v_2 measurements. Based on these results, we used AMPT SM and the cascade mode of UrQMD to cover the full energy range $\sqrt{s_{NN}}$ = 4–11 GeV.

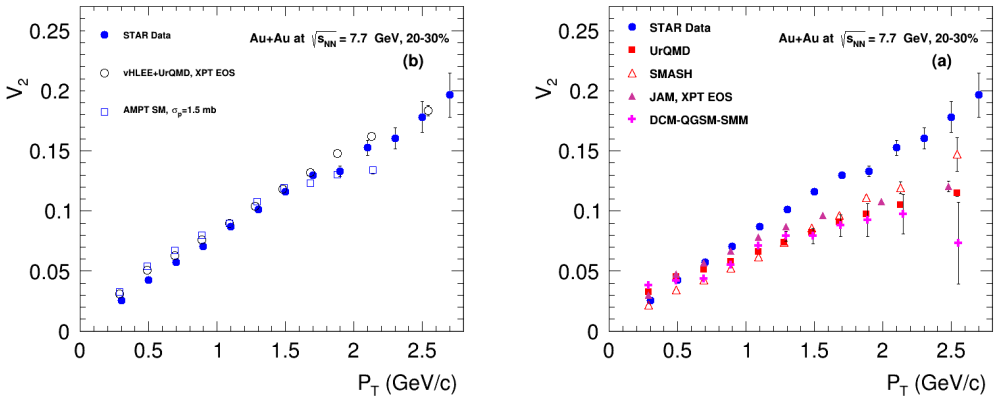

Figure 1. $v_2(p_T)$ of charged hadrons from 20–30% central Au+Au collisions at $\sqrt{s_{NN}}$ = 7.7 GeV. The blue solid circles represent the published $v_2(p_T)$ data from the STAR experiment [20]. The (**b**) shows the prediction of models with QGM formation, including vHLLE+UrQMD and AMPT-SM. The (**a**) shows the pure hadronic transport models (UrQMD, DCM-QGSM-SMM, SMASH, JAM).

The AMPT model [18] is a hybrid model, with the fluctuating initial conditions based on the Heavy-Ion Jet Interaction Generator (HIJING) two-component model. In the string melting version of the AMPT SM model, which is used in the present study, hadrons produced from excited strings in the HIJING model are converted to their valence quarks and antiquarks, and the space-time evolution of QGM evolution is then modeled using Zhang's parton cascade (ZPC) model. At hadronization, quarks and antiquarks in the AMPT model are converted to hadrons via a quark coalescence model; following this, the hadronic interactions are modelled by A Relativistic Transport (ART). We have generated events with the AMPT-SM (version v2.26t7) model with the partonic cross section: σ_p = 1.5 mb, which qualitatively describes the STAR data of $v_2(p_T)$ of charged hadrons at $\sqrt{s_{NN}}$ = 7.7 and 11.5 GeV, Figure 2.

The Ultra-relativistic Quantum Molecular Dynamics (UrQMD) model [17] is a microscopic transport approach based on the binary elastic and inelastic scattering of hadrons, resonance excitations and decays as well as string dynamics and strangeness exchange reactions. We used version 3.4 of the UrQMD with the default set of parameters in the cascade mode.

For each model, a Monte Carlo event sample of 50 millions minimum bias Au + Au collisions has been generated for collision energies $\sqrt{s_{NN}}$ = 5, 7.7, and 11.5 GeV.

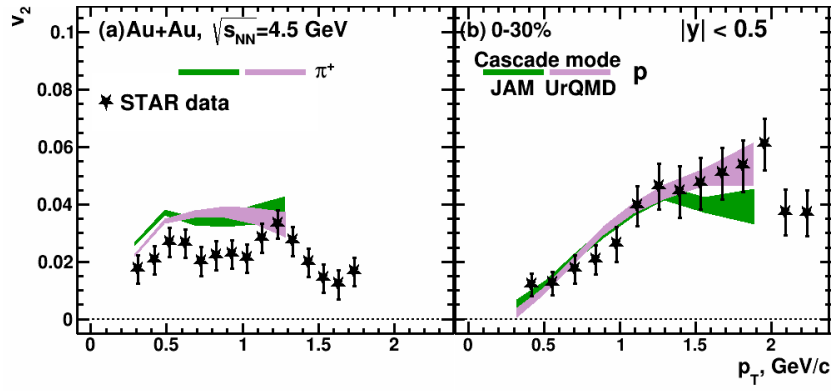

Figure 2. $v_2(p_T)$ of charged pions (**a**) and protons (**b**) in the 0–30% central Au+Au collisions at $\sqrt{s_{NN}}$ = 4.5 GeV. The black closed symbols denote the published data from the STAR experiment [21]. The purple and green bands represent the results from the cascade mode of UrQMD and JAM models, respectively. The figure is taken from [19].

3. Multiplicity-Based Centrality Determination

In this section, we briefly discuss the procedures to determine the centrality of collisions with the Multi-Purpose Detector (MPD) at NICA. The MPD was designed as a 4π spectrometer for detecting charged hadrons, electrons and photons in heavy-ion collisions at high luminosity. In the first stage of operation in 2024, the MPD will consist of the Time Projection Chamber (TPC), the Time-Of-Flight (TOF) detector, the electromagnetic calorimeter (ECal), and the forward hadron calorimeter (FHCal). See the left panel of Figure 3 for further information. TPC will provide 3D tracking of charged particles, as well as measuring the specific ionization energy loss dE/dx to identify the particles with $|\eta| < 1.2$. More details about the detector subsystems of MPD and their performance can be found in [1].

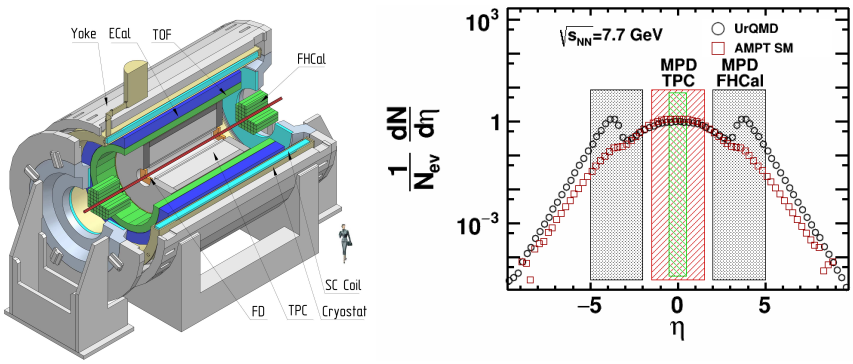

Figure 3. (**left**) The layout of the main detector sub-systems of the MPD experiment in Stage 1. (**right**) Pseudorapidity distributions of charged particles in minimum bias Au+Au collisions at $\sqrt{s_{NN}}$ = 7.7 GeV. Markers represent the event generators: UrQMD (black circles) and AMPT SM (red squares). The pseudorapidity region $|\eta| < 0.5$ of TPC (MPD) used for centrality selection is marked by the green vertical band.

The uncorrected multiplicity of charged particles N_{ch} in the TPC (MPD) is used to determine and define the centrality classes. The pseudorapidity region $|\eta| < 0.5$ of TPC (MPD) used for centrality selection is marked by the green vertical band. See the right part of Figure 3 for further details. The $|\eta|$ range for the multiplicity of charged particles is similar to that used by the STAR experiment for centrality definition during the first Beam Energy Scan program at RHIC: $\sqrt{s_{NN}}$ = 7.7–62.4 GeV [20,22]. The definition of the centrality classes are based on the application of MC Glauber [12,13,28] and Γ-fit [14,15,28] methods.

The present analysis is based on the implementation of the Monte Carlo version of the Glauber model, as described in refs. [11,12]. An input of the MC Glauber model is the nucleon density $\rho(r)$ inside the nucleus. It is usually parametrized by Fermi distribution:

$$\rho(r) = \rho_0 \frac{1 + w\left(\frac{r}{R}\right)^2}{1 + \exp\frac{r-R}{a}}, \tag{2}$$

where R is the radius of the nucleus ($R = R_{Au} = 6.55 \pm 0.05$ fm for ^{197}Au nucleus), the constant ρ_0 corresponds to the density at the center of the nucleus. The skin thickness of the nucleus a defines how abruptly the density falls at the edge of the nucleus ($a = 0.544 \pm 0.010$ fm). The nucleus–nucleus collision is treated as a sequence of independent binary nucleon–nucleon collisions, where the nucleons travel on straight-line trajectories and the inelastic nucleon–nucleon cross section $\sigma_{\mathrm{NN}}^{\mathrm{inel}}$ is assumed to depend only on the collision energy. Two nucleons from different nuclei are assumed to collide if the relative transverse distance d between centers is less than the distance corresponding to the inelastic nucleon–nucleon cross section: $d < \sqrt{\sigma_{\mathrm{NN}}^{\mathrm{inel}}/\pi}$. For selected energies, the values of $\sigma_{\mathrm{NN}}^{\mathrm{inel}}$ are set to 29.4, 29.7, and 31.3 mb for $\sqrt{s_{NN}}$ = 5, 7.7 and 11.5 GeV, correspondingly [29]. The output of the MC Glauber model includes the geometrical properties of the simulated collisions: the impact parameter b, number of binary nucleon–nucleon collisions (N_{coll}), and the number of participating nucleons (N_{part}). The procedure for centrality determination includes fitting experimentally measured particle multiplicity N_{ch} with an MC Glauber model based function $N_{ch}^{fit}(f, \mu, k)$ [12,13,28] :

$$N_{ch}^{fit}(f, \mu, k) = N_a(f) \times P_{\mu,k}, \; N_a(f) = fN_{part} + (1-f)N_{coll}, \tag{3}$$

where $P_{\mu,k}$ is the negative binomial distribution (NBD) with mean μ and width k. $N_a(f)$ is a number of ancestors (number of independent sources), f characterizes the fraction of hard processes, N_{part} and N_{coll} are the number of participants and the number of binary collisions from MC Glauber model output. The optimal set of parameters f, μ and k can be found from the minimization procedure applied to find the minimal value of the χ^2, which is defined as follows:

$$\chi^2 = \sum_{i=n_{low}}^{n_{high}} \frac{\left(F_{fit}^i - F_{data}^i\right)^2}{\left(\Delta F_{fit}^i\right)^2 + \left(\Delta F_{data}^i\right)^2}, \tag{4}$$

where F_{fit}^i and F_{data}^i are values of the fit function and fitted histogram at a given bin i, ΔF_{fit}^i and ΔF_{data}^i are corresponding uncertainties, and n_{low} and n_{high} are the lowest and highest fitting ranges, correspondingly.

For the fit procedure, a 20×10^6 MC Glauber events were generated for each energy point. A grid of k and f parameters was formed with corresponding χ^2 values for each (k,f) combination: $k \in [1, 50]$ with a step of 1 and $f \in [0, 1]$ with a step of 0.01.

As an example, Figure 4 shows the charged particle multiplicity N_{ch} distribution (open squares) for Au+Au collisions at $\sqrt{s_{NN}}$ = 7.7 GeV from the UrQMD (left) and AMPT SM (right) models with overlay fitted distribution using the MC Glauber approach (blue solid triangles). The multiplicities N_{ch} below 15 for UrQMD and 10 for AMPT-SM model events were excluded from the fit. This defines the so-called "anchor point" below which the centrality determination is not reliable. The ratio (N_{ch}^{fit}/N_{ch}) of the fit to the data shows the quality of the procedure, see the bottom part of Figure 4. After finding the optimal set of the fit parameters, one can easily estimate the total cross-section and all events can be divided into groups with a given range of total cross-section (0–10%, 10–20% etc). See the black solid vertical lines in Figure 4 for more information. High multiplicity events have a low average b (central collisions) and low multiplicity events have a large average b

(peripheral collisions). For each centrality class, the mean value of the impact parameter $\langle b \rangle$ and its corresponding standard deviation was found using simulated information from MC Glauber model events.

Figure 5 shows the centrality dependence of $\langle b \rangle$ for UrQMD (left) and AMPT SM (right) model events denoted by open symbols. The $\langle b \rangle$ from the MC Glauber approach (closed symbols) are presented for comparison. The average impact parameter and the width of its distribution estimated with the MC Glauber approach are consistent with the values used in the models by 3–4%, see the bottom plots in Figure 5.

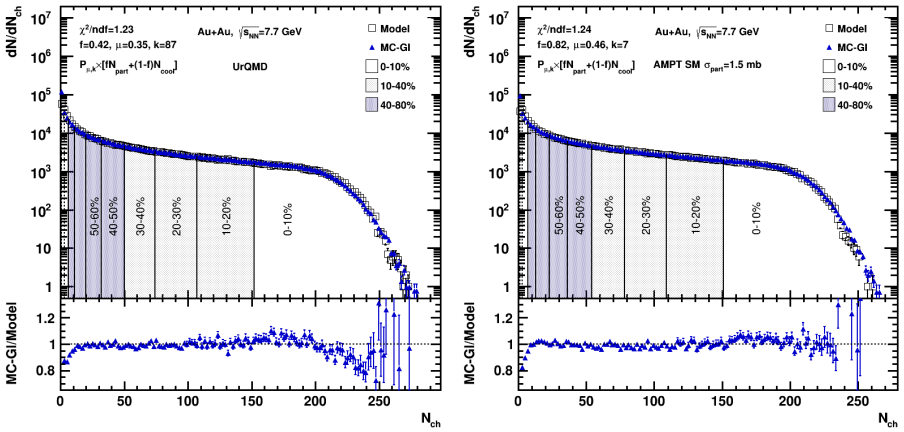

Figure 4. Distributions N_{ch} of charged particles for for Au+Au collisions at $\sqrt{s_{NN}}$ = 7.7 GeV (open symbols). The distributions are fitted with the NBD MC Glauber fit (solid symbols). The results are for the (**left**) and AMPT SM (**right**) model events. The solid vertical lines indicate the resulting centrality classes.

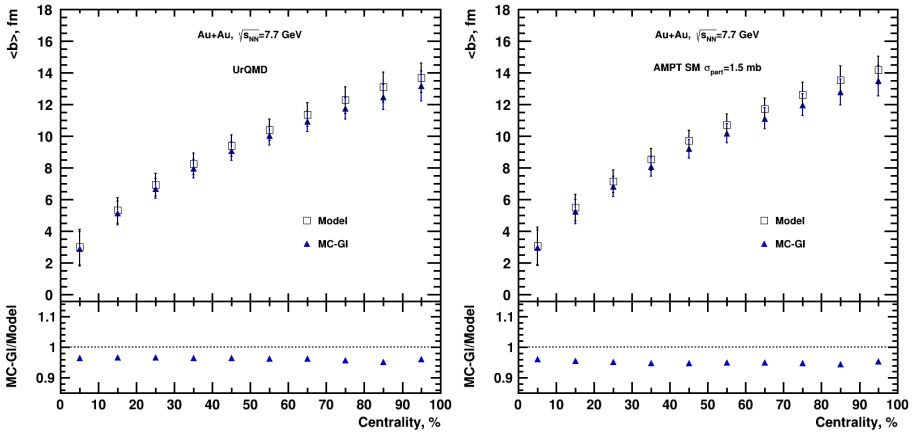

Figure 5. Centrality dependence of the mean value of impact parameter $\langle b \rangle$ for Au+Au collisions at $\sqrt{s_{NN}}$ = 7.7 GeV. The values of $\langle b \rangle$ from the UrQMD (**left**) and AMPT SM (**right**) models (open symbols) are compared with values of MC Glauber model (closed symbols) for the centrality classes defined by NBD fit.

In contrast to the MC Glauber method, the Γ-fit method does not require any modeling of the collision dynamics and can be used over a broad range of collision energies: from $\sqrt{s_{NN}}$ = 5.44 TeV [14,15] to the bombarding energy of 25 AMeV [30]. The method shows that the problem of reconstructing impact parameter b from the measured multiplicity N_{ch} is a typical inverse problem, which can be solved using a deconvolution method. The main element is the fluctuation kernel which is used to model multiplicity fluctuations $P(N_{ch}|b)$

at a fixed impact parameter b. The fluctuations of the multiplicity can be described by the gamma distribution [14,15,28]:

$$P(N_{ch}|b) = \frac{1}{\Gamma(k)\theta^k} N_{ch}^{k-1} e^{-N_{ch}/\theta} \tag{5}$$

where $\Gamma(k)$ is the gamma function and two parameters $k(b)$ and $\theta(b)$ corresponding to the mean, $\langle N_{ch} \rangle$, and to the variance, $\sigma_{N_{ch}}$: $\langle N_{ch} \rangle = k\theta$, $\sigma_{N_{ch}} = \sqrt{k}\theta$. Similar to the multiplicity N_{ch}, which is always positive, the gamma distribution is only defined for $N_{ch} \geq 0$. It can be considered as a continuous version of the negative binomial distribution (NBD), which has long been used to fit multiplicity distributions in heavy-ion collisions [14,15,30]. The normalized measured multiplicity distribution, $P(N_{ch})$, can be obtained by summing the contributions to multiplicity at all impact parameters:

$$P(N_{ch}) = \int_0^\infty P(N_{ch}|b)P(b)db = \int_0^1 P(N_{ch}|c_b)dc_b, \; P(b) = \frac{2\pi b}{\sigma_{inel}} P_{inel}(b), \tag{6}$$

where $P(b)$ is the probability distribution of the impact parameter, and c_b denotes the centrality: $c_b \equiv \int_0^b P(b')db'$. $P(b)$ depends on the probability $P_{inel}(b)$ of an inelastic collision occurring at given b, and σ_{inel} is the inelastic nucleus–nucleus cross section. $P_{inel}(b) \simeq 1$ and $c_b \simeq \pi b^2/\sigma_{inel}$, except for peripheral collisions. For the variable k, one can use the following parameterization:

$$k(c_b) = k_0 \cdot exp\left[-\sum_{i=1}^{3} a_i (c_b)^i\right], \tag{7}$$

we fit $P(N_{ch})$ to the experimental distribution of N_{ch} using Equations (5) and (6) [14,15,28]. The fit for the reconstruction of the probability of N_{ch} at fixed c_b: $P(N_{ch}|c_b)$.

The fitting procedure has been tested for the same charged particle multiplicity N_{ch} distribution from the UrQMD (left) and AMPT SM (right) models, see Figure 6. The result of the Γ-fit is shown as red solid circles. The value of σ_{inel} = 677 fm^2 was used for the Au+Au collision system. In the fit, we exclude values of $N_{ch} < 15$ below the "anchor point" where a fraction of events are missed. We normalized $P(N_{ch})$ in such a way that the fraction of events above the anchor point matches the measured value of N_{ch}. The bottom plots in Figure 6 show the ratio of the resulting fit functions to the charged particle multiplicity distribution. The ratio plots show that the Γ-fit method can reproduce the charged particle multiplicity distribution with good accuracy. Once the probability of N_{ch} at a fixed c_b is reconstructed, the probability distribution of b, at a fixed N_{ch}, can be extracted using Bayes' theorem: $P(b|N_{ch}) = P(N_{ch}|b)P(b)/P(N_{ch})$, where $P(N_{ch}|b) = P(N_{ch}|c_b)$ and $c_b \simeq \pi b^2/\sigma_{inel}$ [14,15,28]. Extending this reconstruction to a finite centrality bin, corresponding to an interval $N_{ch}^{low} < N_{ch} < N_{ch}^{high}$ is straightforward upon integration over N_{ch}:

$$P(b|N_{ch}^{low} < N_{ch} < N_{ch}^{high}) = P(b) \frac{\int_{N_{ch}^{low}}^{N_{ch}^{high}} P(N'_{ch}|b)dN'_{ch}}{\int_{N_{ch}^{low}}^{N_{ch}^{high}} P(N'_{ch})dN'_{ch}}, \tag{8}$$

where $\int_{N_{ch}^{low}}^{N_{ch}^{high}} P(N'_{ch})dN'_{ch}$ is the width of the centrality bin Δc_b (i.e., 0.1 for the 0–10% centrality bin). The 10% centrality classes defined with Γ-fit normalization are indicated with black solid vertical lines in Figure 6.

Figure 7 shows the resulting centrality dependence of the mean value of the impact parameter $\langle b \rangle$ for Au+Au collisions at $\sqrt{s_{NN}}$ = 7.7 GeV. The values of $\langle b \rangle$ extracted from the Γ-fit approach (red solid circles) are compared with the values used in the UrQMD (left) and AMPT SM (right) models denoted by open symbols. The average impact parameter and the width of its distribution estimated with the Γ-fit approach are consistent with the values used in the models by 1–2%.

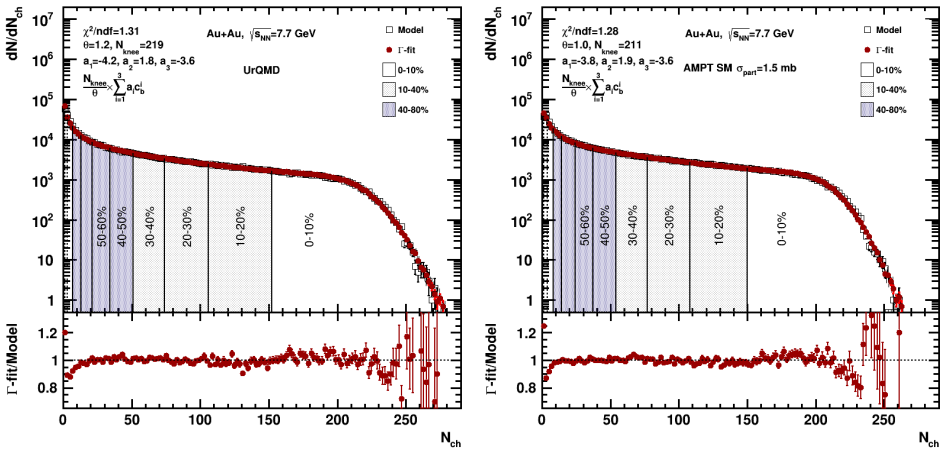

Figure 6. Distributions N_{ch} of charged particles for for Au+Au collisions at $\sqrt{s_{NN}}$ = 7.7 GeV (open symbols). The distributions are fitted with Γ-fit method (solid symbols). The results are for the UrQMD (**left**) and AMPT SM (**right**) model events. The solid vertical lines indicate the resulting centrality classes.

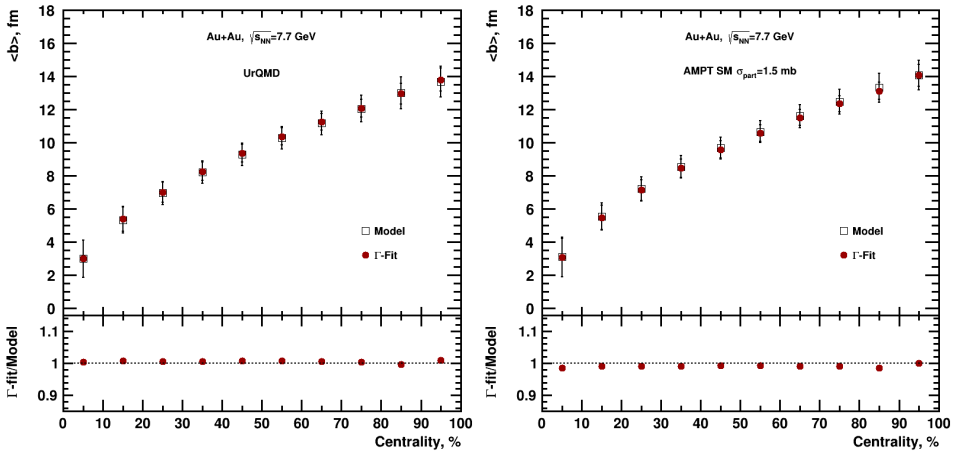

Figure 7. Centrality dependence of the mean value of the impact parameter $\langle b \rangle$ for Au+Au collisions at $\sqrt{s_{NN}}$ = 7.7 GeV. The resulting values of $\langle b \rangle$ extracted from the Γ-fit approach (red solid circles) are compared with the values used in UrQMD (**left**) and AMPT SM (**right**) models denoted by open symbols. Bottom plots show centrality dependence of the ratio of the resulting $\langle b \rangle$ values from the Γ-fit approach to the values from the models.

Results for the Γ-fit approach tend to be in better agreement with model data. However, it should be noted that this approach requires the total integral of the multiplicity distribution to be evaluated separately. Thus, the Γ-fit method is more sensitive to any bias, such as trigger inefficiencies, that could distort the estimation of the total integral of the multiplicity distribution.

4. Methods for Elliptic Flow Measurements

A significant part of the published elliptic flow measurements by the STAR experiment at RHIC, including the Au+Au beam energy scan programs, have been performed using

the traditional events plane and Q-cumulant methods [20–22]. In both cases, the particles detected in the TPC of the STAR experiment ($|\eta| < 1.0$) have been used. In this section, we briefly discuss how the event plane and Q-cumulant methods can be used for the measurements of elliptic flow of the produced particles with an MPD detector system at NICA [31]. Similar to the STAR experiment, the particles detected in the TPC ($|\eta| < 1.5$) of the MPD experiment have been used. The event plane method uses the correlation of the azimuthal angle ϕ of each particle with the azimuthal angle Ψ_n of the event plane reconstructed from the anisotropic flow itself [2]. The event flow vector for elliptic flow (Q_2) and the azimuthal angle of the event plane $\Psi_{2,\mathrm{TPC}}$ can be defined as:

$$Q_{2,x} = \sum_i \omega_i \cos(2\varphi_i),\ Q_{2,y} = \sum_i \omega_i \sin(2\varphi_i), \Psi_{2,TPC} = \frac{1}{2}\tan^{-1}\left(\frac{Q_{2,y}}{Q_{2,x}}\right), \tag{9}$$

where the sum runs over all particles i used in the event plane calculation, and φ_i and ω_i are the laboratory azimuthal angle and the weight for the particle i. The event plane angle $\Psi_{2,\mathrm{TPC}}$ can be used to estimate the magnitude of the elliptic flow $v_2\{EP\}$ signal as follows:

$$v_2\{EP\} = \frac{\langle \cos(2(\phi_i - \Psi_{2,\mathrm{TPC}}))\rangle}{R_2(\Psi_{2,\mathrm{TPC}})} \tag{10}$$

where $R_2(\Psi_{2,\mathrm{TPC}})$ represents the event plane resolution factor.

The cumulants $c_2\{k\}$ can be expressed in terms of the moments of the magnitude of the corresponding flow vector $Q_n \equiv \sum_i^M exp(in\varphi_i)$, where M denotes the multiplicity of selected particles in each event [32]. The single-event average two- and four-particle azimuthal correlations can be expressed as follows [32]:

$$\begin{aligned}
\langle 2\rangle_n &= \langle e^{in(\phi_1-\phi_2)}\rangle = (|Q_n|^2 - M)/(M(M-1)),\\
\langle 4\rangle_n &= \langle e^{in(\phi_1+\phi_2-\phi_3-\phi_4)}\rangle\\
&= \{|Q_n|^4 + |Q_{2n}|^2 - 2\mathrm{Re}[Q_{2n}Q_n^*Q_n^*]\\
&- 2[2(M-2)|Q_{2n}|^2 - M(M-3)]\}\\
&/[M(M-1)(M-2)(M-3)].
\end{aligned} \tag{11}$$

For elliptic flow ($n = 2$), the two- and four-particle cumulants, and the v_2 estimators can be formulated as follows:

$$\begin{aligned}
c_2\{2\} &= \langle\langle 2\rangle\rangle,\\
c_2\{4\} &= \langle\langle 4\rangle\rangle - 2\times\langle\langle 2\rangle\rangle^2,\\
v_2\{2\} &= \sqrt{c_2\{2\}},\\
v_2\{4\} &= \sqrt[4]{-c_2\{4\}}.
\end{aligned} \tag{12}$$

where the double brackets denote the weighted average of multi-particle correlations over all events.

The non-flow effects may affect the results of the v_2 measurements. They are mainly due to the following particle correlations, and not associated with the reaction plane: Bose–Einstein correlations, resonance decays, and momentum conservation. The multi-particle cumulant removes the contribution of non-flow correlations from lower-order correlations [2] and the $v_2\{4\}$ results are expected to be less affected by non-flow effects. In order to suppress non-flow effects in two particle correlation methods: $v_2\{2\}$ and $v_2\{EP\}$, one needs to apply the η-gap ($\Delta\eta > 0.1$) between the two sub-events (see [33] for the details).

Elliptic flow fluctuates from event to event and the magnitude of v_2 fluctuations $\sigma^2_{v2} = \langle v_2^2\rangle - \langle v_2\rangle^2$. Here, the resulting flow signal, averaged over all events, is denoted as

$\langle v_2 \rangle$. In the case of the Q-cumulants ($v_2\{2\}$ and $v_2\{4\}$), for a Gaussian model of fluctuations and in the limit of $\sigma_{v2} \ll \langle v_2 \rangle$, one can write [2]:

$$v_2\{2\} = \langle v_2 \rangle + 0.5 \cdot \sigma^2_{v2}/\langle v_2 \rangle,\ v_2\{4\} = \langle v_2 \rangle - 0.5 \cdot \sigma^2_{v2}/\langle v_2 \rangle. \quad (13)$$

This facilitates investigations of the relative fluctuations of v_2 by the lowest ratio of cumulants $v_2\{4\}/v_2\{2\}$. A large v_2 fluctuation will result in $v_2\{4\}/v_2\{2\} \ll 1$, while a weak one leads to $v_2\{4\}/v_2\{2\} \sim 1$. The eccentricity fluctuations make v_2 in the participant plane larger than in the reaction plane $v_2\{\Psi_{2,\mathrm{TPC}}\} \simeq \langle v_2 \rangle + 0.5 \cdot \sigma^2_{v2}/\langle v_2 \rangle$.

Figure 8 shows the anticipated performance of the MPD experiment for the $v_2(p_T)$ measurements of protons and charged pions in Au+Au collisions at $\sqrt{s_{NN}}$ = 7.7 GeV (upper panels) and $\sqrt{s_{NN}}$ = 11.5 GeV (lower panels) obtained by four-particle cumulants $v_2\{4\}$ (left), two-particle cumulants $v_2\{2\}$ (middle) and TPC event plane $v_2\{\Psi_{2,\mathrm{TPC}}\}$ (right). The agreement between $v_2(p_T$ derived from a fully reconstructed data analysis based on GEANT4 (open symbols) and UrQMD model data (filled symbols) indicate good performance of the MPD for the detailed differential measurements of v_2 [31,33].

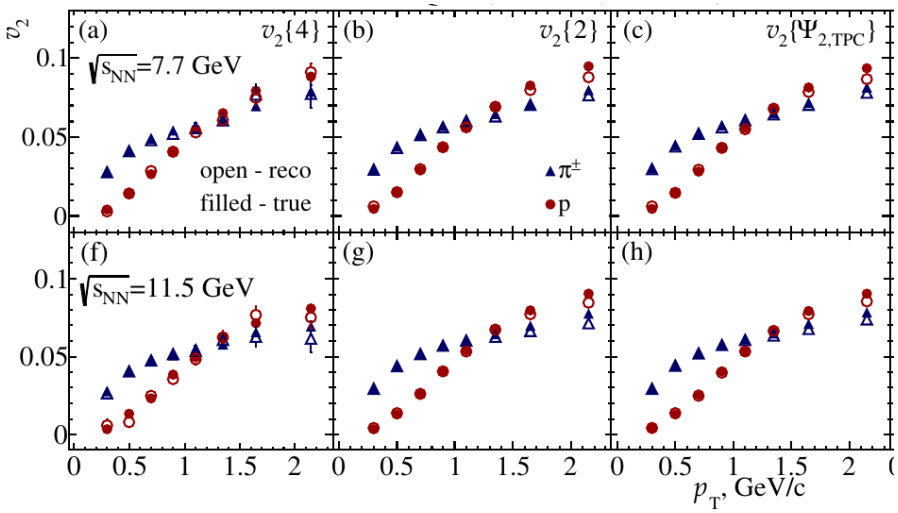

Figure 8. p_T dependence of v_2 of protons (circles) and charged pions (triangles) from 10–40% central Au+Au collisions at $\sqrt{s_{NN}}$ = 7.7 GeV (**a**–**c**) and $\sqrt{s_{NN}}$ = 11.5 GeV (**f**–**h**). (**a**,**f**): four-particle cumulants, two-particle cumulants (**b**,**g**) and TPC event plane (**c**,**h**). The open symbols correspond to the reconstructed data and closed symbols to the UrQMD model data.

5. Results and Discussion

Figures 9 and 10 show the centrality dependence of v_2 of inclusive charged hadrons (0.2< p_T < 3 GeV/c, $|\eta| < 1.5$) from Au+Au collisions at $\sqrt{s_{NN}}$ = 7.7 GeV for UrQMD and AMPT SM model events, respectively. Different symbols correspond to the v_2 results obtained by the different methods of flow measurements: the two particle cumulant $v_2\{2\}$ (circles), four particle cumulant $v_2\{4\}$ (boxes) and event plane $v_2\{EP\}$ (triangles) methods: from left to right. The closed symbols in the figures show the v_2 (impact) results obtained for the centrality procedure based on the impact parameter from the model and the open symbols show the v_2(mult) results for a centrality procedure based on the multiplicity of produced particles: Γ-fit (panel a) and MC Glauber (panel b) approaches, see Section 3 for the details. Bottom plots in each panel of the figure show the centrality dependence of the ratio v_2(impact)/v_2(mult), which can be useful to estimate the centrality selection effect on v_2 measurements. The v_2 signal has a maximum value in 20–40% mid-central collisions, where it practically does not change. It decreases for both peripheral and central collisions, as shown in Figures 9 and 10. Based on this observation, one can expect that the centrality selection will affect mostly the results of v_2 measurements in central and peripheral collisions. The v_2(impact) results obtained for the centrality procedure based on the impact parameter from the model and v_2(mult) results obtained

for centrality procedure based on the multiplicity of produced particles using the Γ-fit approach are found to be in a good agreement, excluding the 0–10% of central collisions. Here, $v_2(\text{impact}) < v_2(\text{mult})$ by 4–5%. For the MC Glauber approach, the difference between v_2(impact) and v_2(mult) is larger (up to 8–10%) and it has a strong centrality dependence. See panel (b) in Figures 9 and 10 for more information.

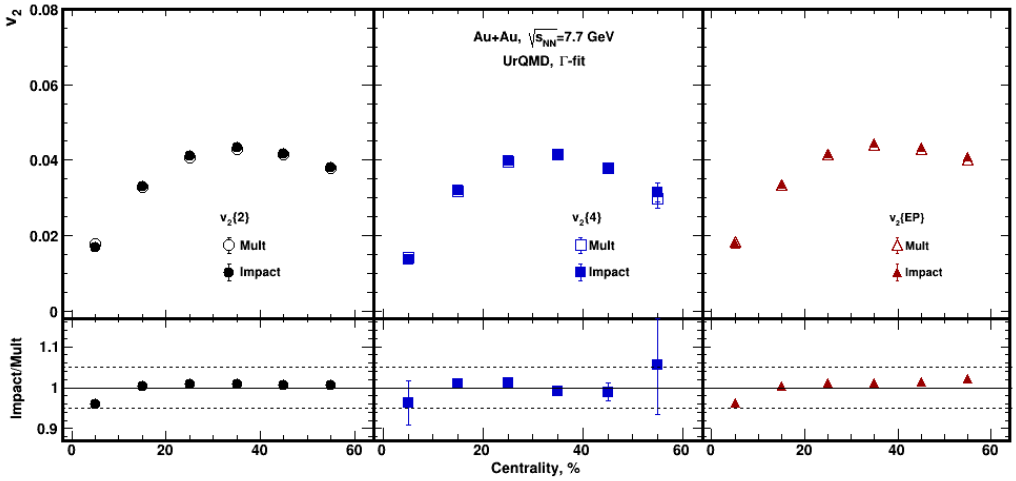

(**a**)

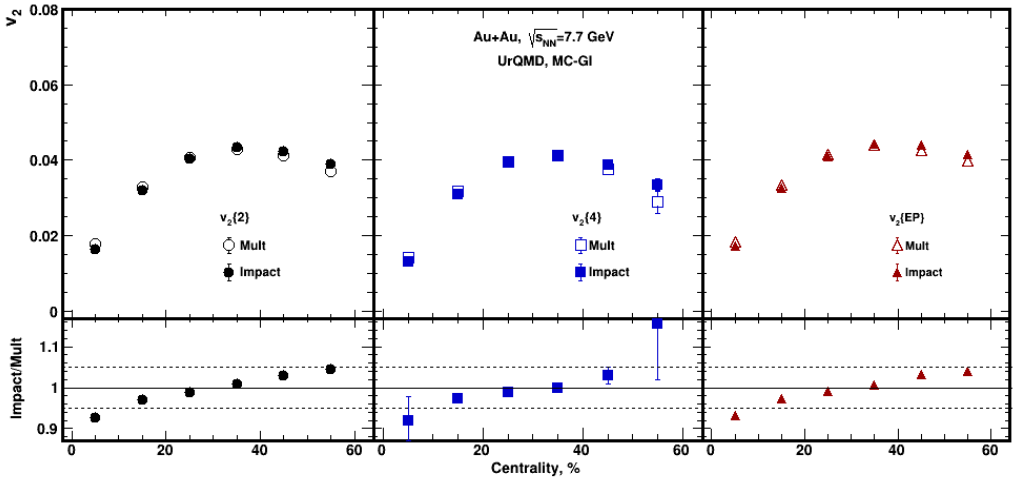

(**b**)

Figure 9. Centrality dependence of v_2 of inclusive charged hadrons from the UrQMD model for Au+Au collisions at $\sqrt{s_{NN}} = 7.7$ GeV. Different symbols correspond to the v_2 results obtained by the two particle cumulant $v_2\{2\}$ (circles), four particle cumulant $v_2\{4\}$ (boxes) and event plane $v_2\{EP\}$ (triangles) methods: from left to right. The closed symbols show the v_2(impact) results obtained for the centrality procedure based on the impact parameter from the model and the open symbols show v_2(mult) for the centrality procedure based on the multiplicity of produced particles: Γ-fit (**a**) and MC Glauber (**b**) approaches. Bottom plots in each panel show the centrality dependence of the ratio $v_2(\text{impact})/v_2(\text{mult})$.

The larger difference between v_2 (impact) and v_2(mult) for MC Glauber approach results from the systematic shift between the $\langle b \rangle$ and the model data. See Section 3 for more information.

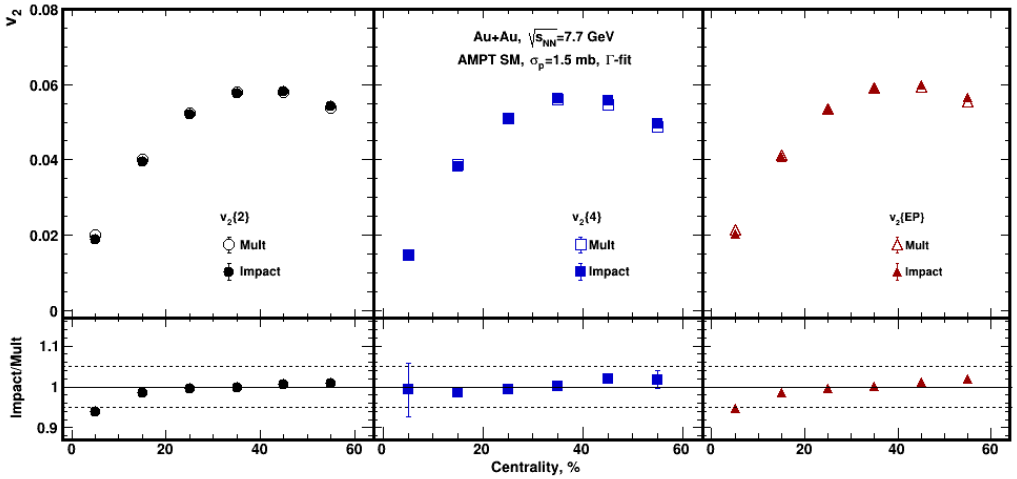

(**a**)

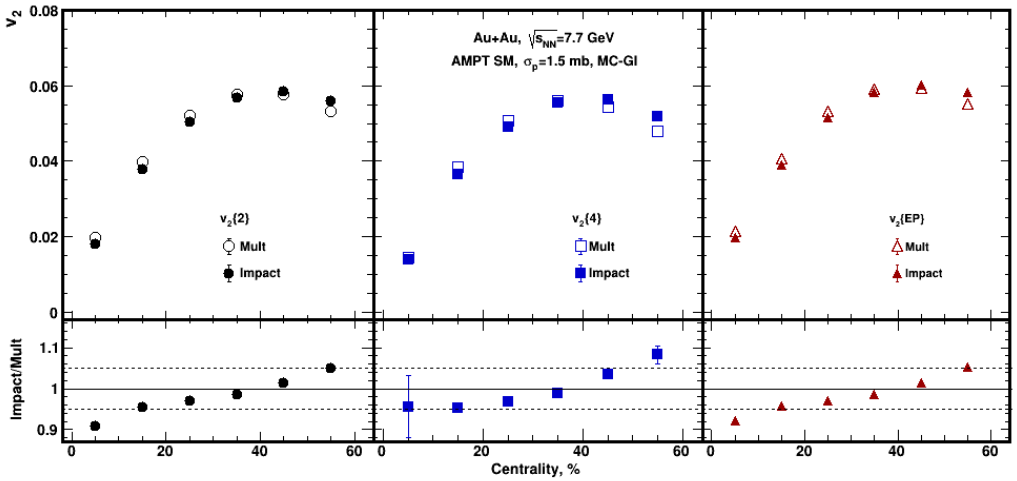

(**b**)

Figure 10. Centrality dependence of v_2 of inclusive charged hadrons from the AMPT SM model for Au+Au collisions at $\sqrt{s_{NN}} = 7.7$ GeV. Different symbols correspond to the v_2 results obtained by the two particle cumulant $v_2\{2\}$ (circles), four particle cumulant $v_2\{4\}$ (boxes) and event plane $v_2\{EP\}$ (triangles) methods: from left to right. The closed symbols show the v_2(impact) results obtained for the centrality procedure based on the impact parameter from the model and the open symbols show v_2(mult) for the centrality procedure based on the multiplicity of produced particles: Γ-fit (**a**) and MC Glauber (**b**) approaches. Bottom plots in each panel show the centrality dependence of the ratio v_2(impact)/v_2(mult).

The difference between v_2(impact) and v_2(mult) does not depend on the flow measurement method and is the same for models UrQMD and AMPT SM. Figures 11–13 show the centrality dependence of v_2 of inclusive charged hadrons from the UrQMD model for Au+Au collisions at $\sqrt{s_{NN}}$ = 5 GeV (left), 7.7 GeV (center) and 11.5 GeV (right). The results are presented for two particle cumulant $v_2\{2\}$ (circles), four particle cumulant $v_2\{4\}$ (boxes) and event plane $v_2\{EP\}$ (triangles) methods. The closed symbols show the v_2(impact) results obtained for the centrality procedure based on the impact parameter from the model and the open symbols show the v_2(mult) for the centrality procedure based on the multiplicity of produced particles: Γ-fit (panel a) and MC Glauber (panel b) approaches. The general trends for the difference between v_2(impact) and v_2(mult) are very similar to those observed for $\sqrt{s_{NN}}$ = 7.7 GeV, see Figures 9 and 10. However, the difference increases with decreasing the collision energy from $\sqrt{s_{NN}}$ = 11.5 GeV to 5 GeV for all methods of elliptic flow measurements.

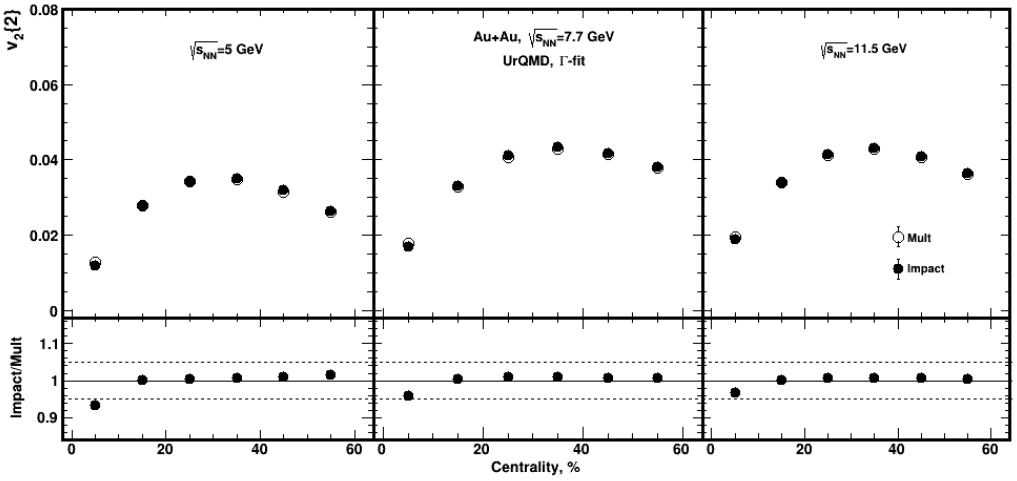

(**a**)

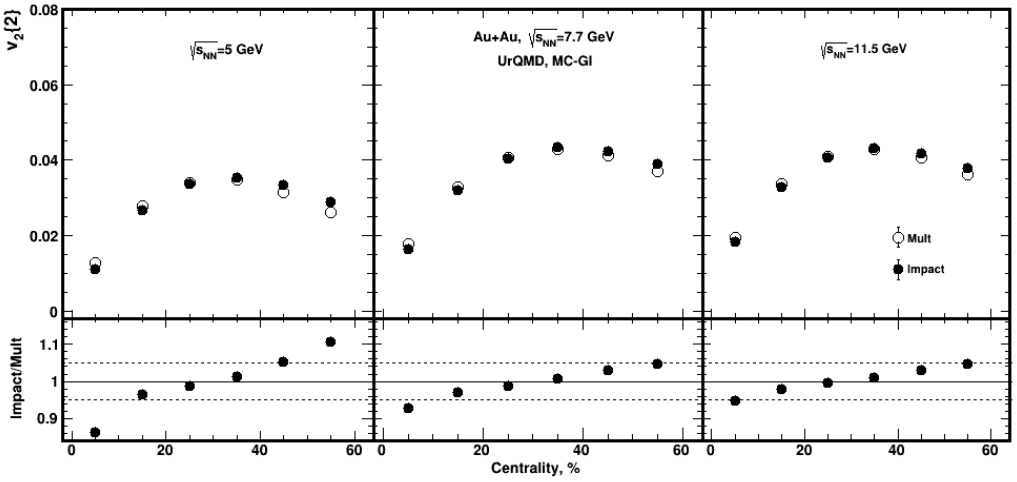

(**b**)

Figure 11. Centrality dependence of $v_2\{2\}$ of inclusive charged hadrons from the UrQMD model for Au+Au collisions at $\sqrt{s_{NN}}$ = 5 GeV (left), 7.7 GeV (center) and 11.5 GeV (right). The closed symbols show the v_2(impact) results obtained for the centrality procedure based on the impact parameter from the model and the open symbols show the v_2(mult) for the centrality procedure based on the multiplicity of produced particles: Γ-fit (**a**) and MC Glauber (**b**) approaches. Bottom plots in each panel show the centrality dependence of the ratio v_2(impact)/v_2(mult).

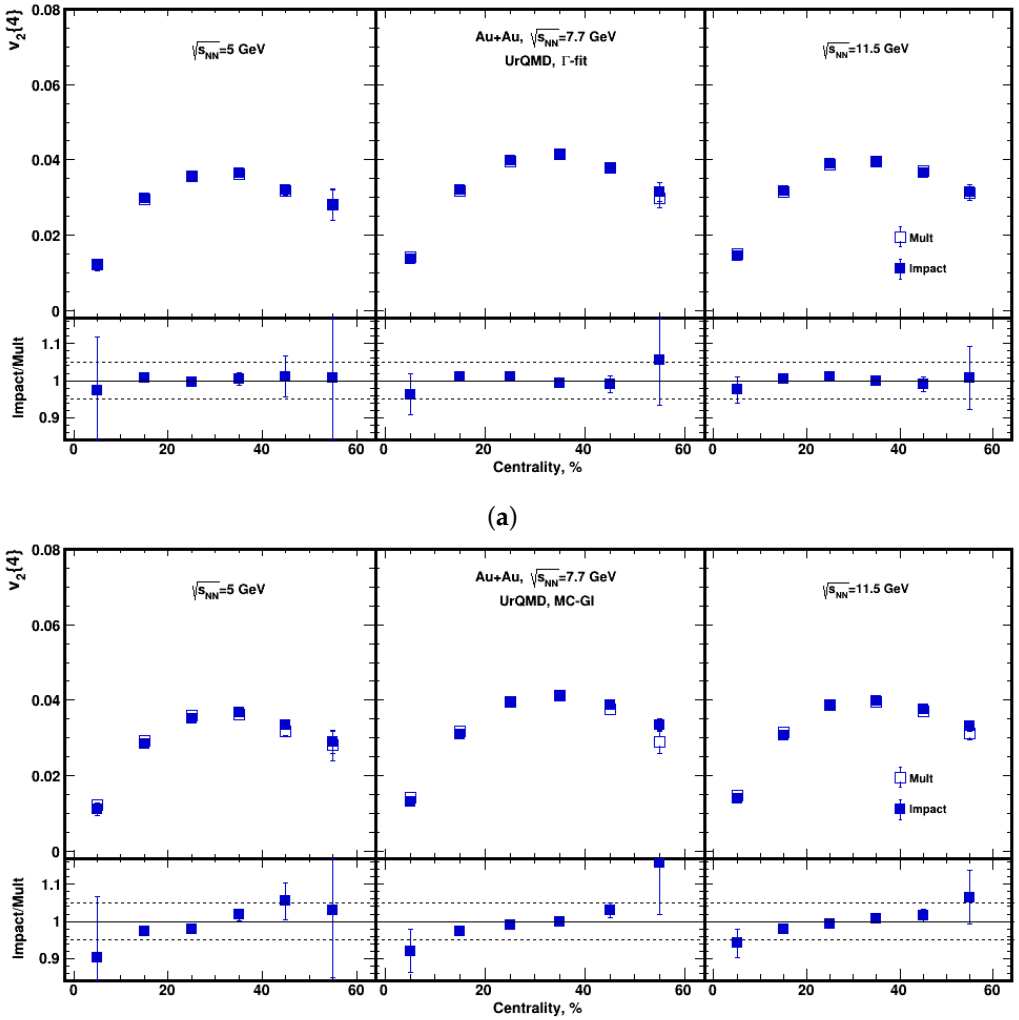

Figure 12. Centrality dependence of $v_2\{4\}$ of inclusive charged hadrons from the UrQMD model for Au+Au collisions at $\sqrt{s_{NN}}$ = 5 GeV (**left**), 7.7 GeV (**center**) and 11.5 GeV (**right**). The closed symbols show the v_2(impact) results obtained for the centrality procedure based on the impact parameter from the model and open symbols show the v_2(mult) for the centrality procedure based on the multiplicity of produced particles: Γ-fit (**a**) and MC Glauber (**b**) approaches. Bottom plots in each panel show the centrality dependence of the ratio v_2(impact)/v_2(mult).

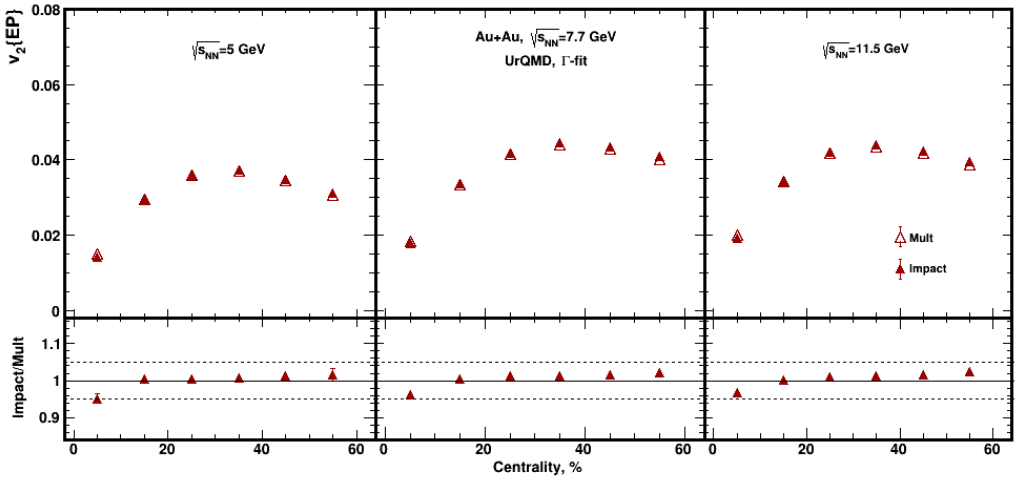

(**a**)

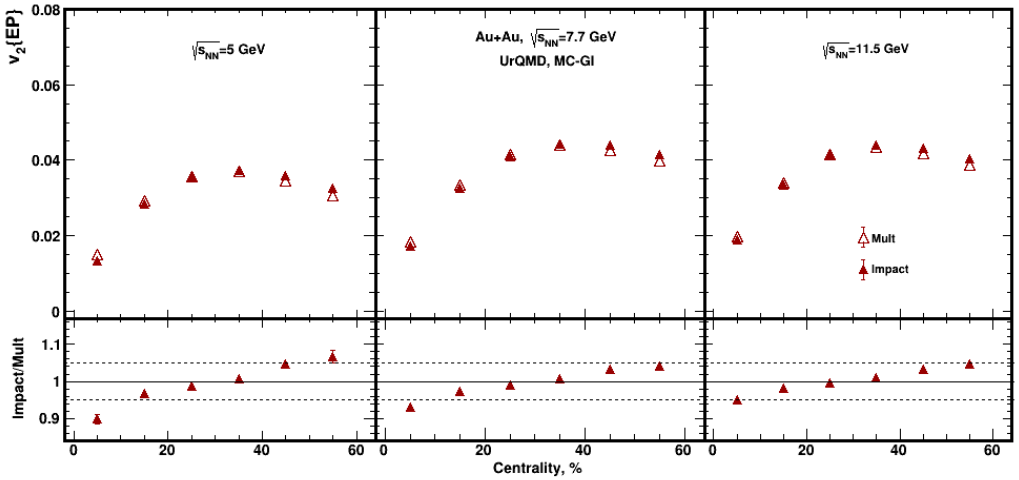

(**b**)

Figure 13. Centrality dependence of $v_2\{EP\}$ of inclusive charged hadrons from the UrQMD model for Au+Au collisions at $\sqrt{s_{NN}}$ = 5 GeV (**left**), 7.7 GeV (**center**) and 11.5 GeV (**right**). The closed symbols show the v_2(impact) results obtained for the centrality procedure based on the impact parameter from the model and the open symbols show the v_2(mult) for the centrality procedure based on the multiplicity of produced particles: Γ-fit (**a**) and MC Glauber (**b**) approaches. Bottom plots in each panel show the centrality dependence of the ratio v_2(impact)/v_2(mult).

Figure 14 shows the centrality dependence of the ratio $v_2\{4\}/v_2\{2\}$ of inclusive charged hadrons from the UrQMD model for Au+Au collisions at $\sqrt{s_{NN}}$ = 5 GeV (left), 7.7 GeV (center) and 11.5 GeV (right). The centrality selection effect does not change the ratio $v_2\{4\}/v_2\{2\}$, as it acts in a similar way for $v_2\{2\}$ and $v_2\{4\}$ results.

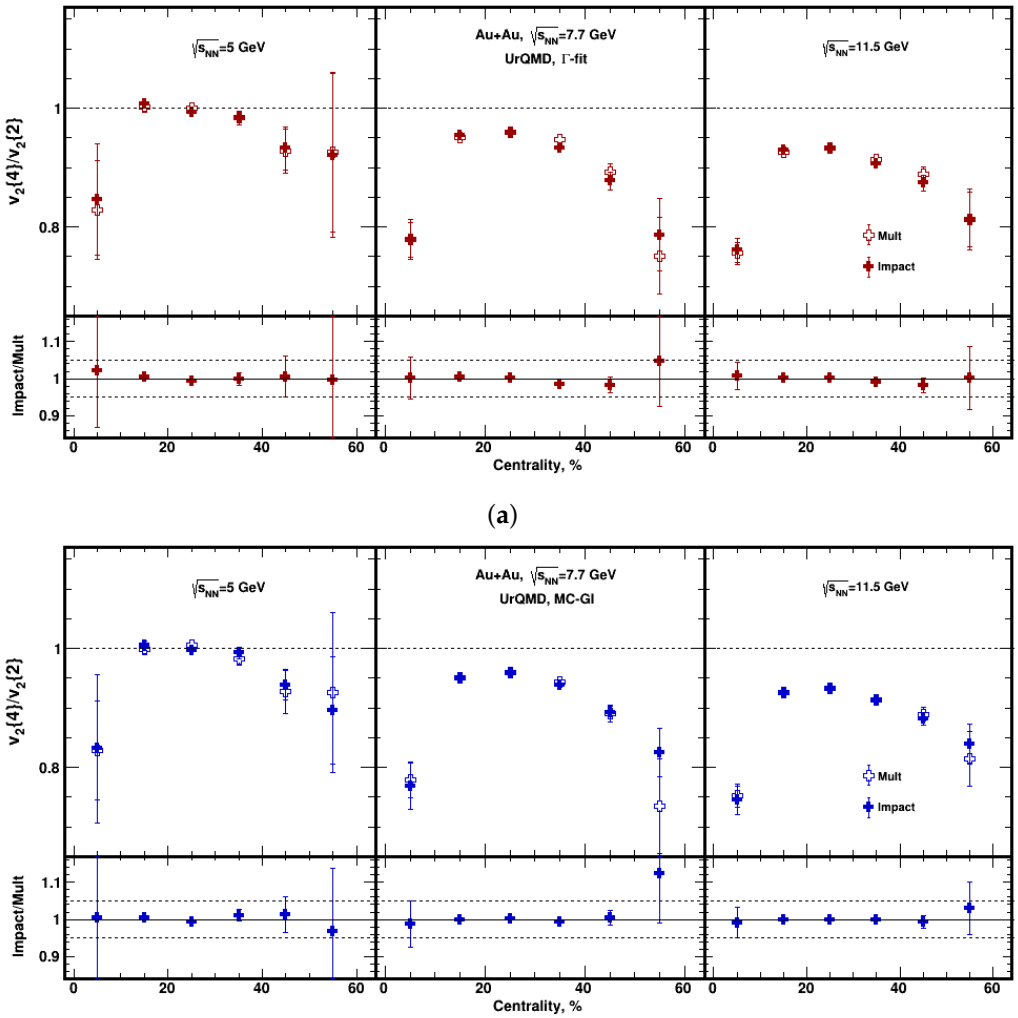

Figure 14. Centrality dependence of the ratio $v_2\{4\}/v_2\{2\}$ of inclusive charged hadrons from the UrQMD model for Au+Au collisions at $\sqrt{s_{NN}}$ = 5 GeV (**left**), 7.7 GeV (**center**) and 11.5 GeV (**right**). The closed symbols show the results obtained for the centrality procedure based on the impact parameter obtained from the model and the open symbols show results for the centrality procedure based on the multiplicity of produced particles: Γ-fit (**a**) and MC Glauber (**b**) approaches. Bottom plots in each panel show the centrality dependence of the ratio of the results (impact)/(mult).

6. Conclusions

In summary, we have studied the effects of different methods used for the centrality selection on the elliptic flow measurements in Au+Au collisions at $\sqrt{s_{NN}}$ = 5 GeV, 7.7 and 11.5 GeV within the framework of the cascade version of UrQMD and string melting version of AMPT-SM models. The centralities were defined by the charged-particle multiplicities of produced particles. The elliptic flow v_2(mult) results from events with centrality classes defined using the MC Glauber and Γ-fit approaches have been compared to v_2(impact) with centrality classes based on the true impact parameter from the models. The difference between v_2(impact) and v_2(mult) is around 1–2% for the Γ-fit approach, except for central collisions where the difference is 4–5%. For the MC Glauber approach, the difference between v_2(impact) and v_2(mult) is larger (up to 8–10%) and it has a strong centrality dependence. The v_2 difference increases with decreasing collision energy from $\sqrt{s_{NN}}$ = 11.5 GeV to 5 GeV for all methods of elliptic flow measurements, used in the present work. The results indicate that the data-driven and model independent Γ-fit approach provides a more accurate way to reconstruct the impact parameter than the model-dependent MC

Glauber method. As a result, the centrality selection by the Γ-fit approach will only slightly affect the results of v_2 measurements in 0–10% of central collisions, where the v_2 signal is very small and strongly depends on centrality.

Our work may serve as a baseline for the centrality selection of the elliptic flow in the future relativistic heavy-ion collision experiments at NICA energies. In the future, we plan to include the other estimators of centrality based on spectator fragments and extend the study to other flow harmonics.

Author Contributions: Software, D.I.; Validation, P.P.; Formal analysis, D.I.; Investigation, D.I.; Writing—original draft, D.I.; Supervision, P.P., Funding, Project Administration, Writing—review and editing, A.T. All authors have read and agreed to the published version of the manuscript.

Funding: This work was funded by the MEPhI program Priority 2030 and by the Ministry of Science and Higher Education of the Russian Federation, Project "New Phenomena in Particle Physics and the Early Universe" No FSWU-2023-0073. Part of this research by P. Parfenov was done in INR RAS and is supported by RSF grant No. 22-12-00132.

Institutional Review Board Statement: Not applicable.

Informed Consent Statement: Not applicable.

Data Availability Statement: Not applicable.

Acknowledgments: Computations were held on the basis of the HybriLIT heterogeneous computing platform (MLIT, JINR).

Conflicts of Interest: The authors declare no conflict of interest. The funders had no role in the design of the study; in the collection, analyses, or interpretation of data; in the writing of the manuscript, or in the decision to publish the results.

References

1. Abgaryan, V.; Acevedo Kado, R.; Afanasyev, S.V.; Agakishiev, G.N.; Alpatov, E.; Altsybeev, G.; Alvarado Hernandez, M.; Andreeva, S.V.; Andreeva, T.V.; Andronov, E.V.; et al. Status and initial physics performance studies of the MPD experiment at NICA. *Eur. Phys. J. A* **2022**, *58*, 140. [CrossRef]
2. Voloshin, S.A.; Poskanzer, A.M.; Snellings, R. Collective phenomena in non-central nuclear collisions. *Landolt-Bornstein* **2010**, *23*, 293. [CrossRef]
3. Ritter, H.G.; Stock R. Collective Flow of QCD Matter: A Historical Introduction. *J. Phys. G* **2014**, *41*, 124002. [CrossRef]
4. Busza, W.; Rajagopal, K.; Schee, W. Heavy Ion Collisions: The Big Picture, and the Big Questions. *Ann. Rev. Nucl. Part. Sci.* **2018**, *68*, 339–376. [CrossRef]
5. Bernhard, J.E.; Moreland, J.S.; Bass, S.A. Bayesian estimation of the specific shear and bulk viscosity of quark-gluon plasma. *Nature Phys.* **2019** *15*, 1113–1117. [CrossRef]
6. Qiu, Z.; Heinz, U.W. Event-by-event shape and flow fluctuations of relativistic heavy-ion collision fireballs. *Phys. Rev.* **2011**, *C84*, 024911. [CrossRef]
7. Niemi, H.; Denicol, G.S.; Holopainen, H.; Huovinen, P. Event-by-event distributions of azimuthal asymmetries in ultrarelativistic heavy-ion collisions. *Phys. Rev.* **2013**, *C87*, 054901. [CrossRef]
8. Gardim, F.G.; Noronha-Hostler, J.; Luzum, M.; Grassi, F.; Ollitrault, J.-Y. Effects of viscosity on the mapping of initial to final state in heavy ion collisions. *Phys. Rev.* **2015**, *C91*, 034902. [CrossRef]
9. Broniowski, W.; Florkowski, W. Geometric relation between centrality and the impact parameter in relativistic heavy ion collisions. *Phys. Rev. C* **2002**, *65*, 024905. [CrossRef]
10. Tarafdar, S.; Citron, Z.; Milov, A. A Centrality Detector Concept. *Nucl. Instrum. Meth. A* **2014**, *768*, 170–178. [CrossRef]
11. Loizides, C.; Nagle, J.; Steinberg, P. Improved version of the PHOBOS Glauber Monte Carlo. *SoftwareX* **2015**, *1–2*, 13. [CrossRef]
12. Abelev, B.; Adam, J.; Adamova, D.; Adare, A.M.; Aggarwal, M.M.; Rinella, G.A.; Agnello, M.; Agocs, A.G.; Agostinelli, A.; Ahammed, Z.; et al. Centrality determination of Pb-Pb collisions at $\sqrt{s_{NN}}$ = 2.76 TeV with ALICE. *Phys. Rev. C* **2013**, *88*, 044909. [CrossRef]
13. Klochkov, V.; Selyuzhenkov, I. Centrality Determination in Heavy-ion Collisions with CBM. *Acta Phys. Pol. B Proc. Suppl.* **2017**, *10*, 919. [CrossRef]
14. Rogly, R.; Giacalone, G.; Ollitrault, J.Y. Reconstructing the impact parameter of proton-nucleus and nucleus-nucleus collisions. *Phys. Rev. C* **2018**, *98*, 024902. [CrossRef]
15. Das, S.J.; Giacalone, G.; Monard, P.A.; Ollitrault, J.Y. Relating centrality to impact parameter in nucleus-nucleus collisions. *Phys. Rev. C* **2018**, *97*, 014905. [CrossRef]

16. Demanov, A.; Parfenov, P.; Taranenko, A. Evolution of elliptic flow of produced particles from Au+Au collisions at $\sqrt{s_{NN}}$=4.5−200 Gev in a hybrid model. *AIP Conf. Proc.* **2021**, *2377*, 030003. [CrossRef]
17. Bass, S.A.; Belkacem, M.; Bleicher, M.; Brandstetter, M.; Bravina, L.; Ernst, C.; Gerland, L.; Hofmann, M.; Hofmann, S.; Konopka, J.; et al. Microscopic models for ultrarelativistic heavy ion collisions. *Prog. Part. Nucl. Phys.* **1998**, *41*, 255–369. [CrossRef]
18. Lin, Z.W.; Ko, C.M.; Li, B.A.; Zhang, B.; Pal, S. A Multi-phase transport model for relativistic heavy ion collisions. *Phys. Rev. C* **2005**, *72*, 064901. [CrossRef]
19. Parfenov P. Model Study of the Energy Dependence of Anisotropic Flow in Heavy-Ion Collisions at $\sqrt{s_{NN}}$ = 2–4.5 GeV. *Particles* **2022**, *5*, 561–579. [CrossRef]
20. Adamczyk, L.; Agakishiev, G.; Aggarwal, M.M.; Ahammed, Z.; Alakhverdyants, A.V.; Alekseev, I.; Alford, J.; Anderson, B.D.; Anson, C.D.; Arkhipkin, D.; et al. Inclusive charged hadron elliptic flow in Au + Au collisions at $\sqrt{s_{NN}}$ = 7.7–39 GeV. *Phys. Rev. C* **2012**, *86*, 054908. [CrossRef]
21. Abdallah, M.S.; Adam, J.; Adamczyk, L.; Adams, J.R.; Adkins, J.K.; Agakishiev, G.; Aggarwal, I.; Aggarwal, M.M.; Ahammed, Z.; Alekseev, I.; et al. Flow and interferometry results from Au+Au collisions at $\sqrt{s_{NN}}$ = 4.5 GeV. *Phys. Rev. C* **2021**, *103*, 034908. [CrossRef]
22. Adamczyk, L.; Adkins, J.K.; Agakishiev, G.; Aggarwal, M.M.; Ahammed, Z.; Alekseev, I.; Alford, J.; Anson, C.D.; Aparin, A.; Arkhipkin, D.; et al. Elliptic flow of identified hadrons in Au+Au collisions at $\sqrt{s_{NN}}$ = 7.7–62.4 GeV. *Phys. Rev. C* **2013**, *88*, 014902. [CrossRef]
23. Karpenko, I.-A.; Huovinen, P.; Bleicher, M. A 3+1 dimensional viscous hydrodynamic code for relativistic heavy ion collisions, *Comput. Phys. Commun.* **2014**, *185*, 3016–3027. [CrossRef]
24. Karpenko, I.-A.; Huovinen, P.; Petersen, H.; Bleicher, M. Estimation of the shear viscosity at finite net-baryon density from $A + A$ collision data at $\sqrt{s_{\rm NN}} = 7.7 - 200$ GeV, *Phys. Rev. C* **2015**, *91*, 064901. [CrossRef]
25. Baznat, A.; Botvina, A.; Musulmanbekov, G.; Toneev, V.; Zhezher, V.; Monte-Carlo Generator of Heavy Ion Collisions DCM-SMM. *Phys. Part. Nucl. Lett.* **2020**, *17*, 303–324. [CrossRef]
26. Nara, Y.; JAM: An event generator for high energy nuclear collisions. *EPJ Web Conf.* **2019**, *208*, 11004. [CrossRef]
27. Weil, J.; Steinberg, V.; Staudenmaier, J.; Pang, L.G.; Oliinychenko, D.; Mohs, J.; Kretz, M.; Kehrenberg, T.; Goldschmidt, A.; Bauchle, B.; et al. Particle production and equilibrium properties within a new hadron transport approach for heavy-ion collisions. *Phys. Rev. C* **2016**, *94*, 054905. [CrossRef]
28. Parfenov, P.; Idrisov, D.; Luong, V.B.; Taranenko, A. Relating Charged Particle Multiplicity to Impact Parameter in Heavy-Ion Collisions at NICA Energies. *Particles* **2021**, *4*, 275–287. [CrossRef]
29. Data Files and Plots of Cross-Sections and Related Quantities in the 2018 Review of Particle Physics. 2018. Available online: https://pdg.lbl.gov/2018/hadronic-xsections/hadron.html (accessed on 22 March 2023).
30. Frankl, J.D.; Gruyer, D.; Bonnet, E.; Borderie, B.; Bougault, R.; Chbihi, A.; Ducret, J.E.; Dur, D.; Fable, Q.; Henri, M.; et al. Model independent reconstruction of impact parameter distributions for intermediate energy heavy ion collisions. *Phys. Rev. C* **2021**, *104*, 034609. [CrossRef]
31. Idrisov, D.; Luong, V.B.; Geraksiev, N.; Demanov, D.; Parfenov, P.; Taranenko, A. Methods for Elliptic Flow Measurements with the MPD Experiment at NICA. *Phys. Part. Nucl.* **2021**, *52*, 637–643. [CrossRef]
32. Bilandzic, A.; Snellings, R.; Voloshin, S. Flow analysis with cumulants: Direct calculations. *Phys. Rev. C* **2011**, *83*, 044913. [CrossRef]
33. Luong, V.B.; Idrisov, D.; Parfenov, P.; Taranenko, A. Elliptic Flow and Its Fluctuations from Transport Models for Au+Au Collisions at $\sqrt{s_{NN}}$ = 7.7 and 11.5 GeV. *Particles* **2023**, *6*, 17–29. [CrossRef]